GEOPHYSICS, VOL. 76, NO. 3 (MAY-JUNE 2011); P. WA23–WA29, 5 FIGS., 6 TABLES.
10.1190/1.3552690

Moveout inversion of wide-azimuth P-wave data for tilted TI media

Xiaoxiang Wang[1] and Ilya Tsvankin[1]

ABSTRACT

Currently TTI (transversely isotropic with a tilted symmetry axis) models are widely used for velocity analysis and imaging in many exploration areas. We develop a 3D parameter-estimation algorithm for TTI media composed of homogeneous layers separated by plane dipping interfaces. The input data include P-wave NMO ellipses and time slopes (horizontal slownesses of the zero-offset rays) combined with borehole information. If the symmetry axis is perpendicular to the bottom of each layer, it is possible to estimate the interval symmetry-direction velocity V_{P0}, anisotropy parameter δ, and the reflector orientation using a single constraint — the reflector depth. The algorithm can tolerate small $(\leq 5^\circ)$ deviation of the symmetry axis from the reflector normal. However, as is the case for the 2D problem, the parameter ε can seldom be obtained without nonhyperbolic moveout inversion. If the symmetry axis deviates from the reflector normal but is confined to the dip plane, stable parameter estimation requires specifying a relationship between the tilt and dip in each layer. When the tilt represents a free parameter, the input data have to be supplemented by wide-azimuth VSP traveltimes with the offset reaching at least 1/4 of the maximum reflector depth. Moreover, the additional angle coverage provided by VSP data may help resolve the parameter ε in the upper part of the model. The developed methodology can be used to build an accurate initial anisotropic velocity model for processing of wide-azimuth surveys.

INTRODUCTION

Transversely isotropic media with a tilted symmetry axis (TTI) provide marked improvements in prestack imaging of P-wave data (Charles et al., 2008; Huang et al., 2008; Neal et al., 2009). Allowing for the symmetry-axis tilt results in more plausible velocity models for sedimentary formations in complex geological settings including fold-and-thrust belts and subsalt plays (Vestrum et al., 1999; Behera and Tsvankin, 2009; Bakulin et al., 2010).

P-wave velocities and traveltimes in TTI media can be expressed through the symmetry-direction velocity V_{P0} and Thomsen (1986) anisotropy parameters ε and δ defined with respect to the symmetry axis. The symmetry-axis orientation is specified by the tilt angle ν with the vertical and the azimuth β. Although many migration algorithms have been extended to TTI media, accurate estimation of the interval anisotropy parameters and the symmetry-axis orientation remains a difficult problem.

For example, Grechka et al. (2001) discuss 2D inversion of P-wave normal-moveout (NMO) velocities and zero-offset traveltimes for the parameters of a dipping TTI layer with the symmetry axis perpendicular to the bedding. Their algorithm is based on several a priori assumptions about the model and requires reflection data from a horizontal interface beneath the TTI layer. Joint moveout inversion of wide-azimuth PP and PS (or SS) reflection data for layered TI media with arbitrary symmetry-axis orientation is developed by Grechka et al. (2002a). Despite the addition of shear-wave traveltimes, parameter estimation is well-posed only for relatively large tilts ν and reflector dips.

A review of several other velocity-analysis algorithms for TTI media can be found in our previous publication (Wang and Tsvankin, 2010), where we develop a 2D inversion methodology for a stack of homogeneous TTI layers separated by plane dipping interfaces. P-wave NMO velocities, reflection slopes, and zero-offset traveltimes are supplemented with reflector depths measured in a borehole, as well as with check-shot and near-offset VSP traveltimes. Even for a single TTI layer, the medium parameters cannot be resolved without a priori knowledge of the tilt of the symmetry axis. Therefore, the symmetry axis is assumed to be orthogonal to the layer's bottom, which is typical for dipping shale layers (Isaac and Lawton, 1999; Vestrum et al., 1999; Charles et al., 2008). Then the 2D algorithm with borehole constraints produces stable estimates of the interval parameters V_{P0} and δ for models with a limited range of interface dips.

Manuscript received by the Editor 30 July 2010; revised manuscript received 25 October 2010; published online 23 May 2011.
[1]Colorado School of Mines, Center for Wave Phenomena, Geophysics Department, Golden, Colorado, U.S.A. E-mail: xwang@mines.edu; ilya@dix.mines.edu.

Here, we present a 3D extension of the inversion algorithm of Wang and Tsvankin (2010) by including the NMO ellipses and two horizontal slownesses of the zero-offset rays (reflection time slopes) in the objective function. Additional information provided by wide-azimuth data makes it possible to relax the constraints on model geometry and increase the stability of the inversion. First, we discuss 3D parameter estimation for models with the symmetry axis orthogonal to reflectors. Then we extend the method to media with arbitrary tilt and show that stable inversion requires the addition of VSP data. The accuracy and stability of estimating the interval TTI parameters for different types of input data is evaluated using synthetic tests on noise-contaminated data.

3D INPUT DATA VECTOR

As in our previous paper (Wang and Tsvankin, 2010), we consider a stack of homogeneous TTI layers separated by plane, dipping, nonintersecting boundaries (Figure 1). However, the dip planes of model interfaces no longer have to be aligned. From 3D multiazimuth P-wave data recorded at a common midpoint (CMP) with the coordinates $\mathbf{Y}=[\mathrm{Y}_1,\mathrm{Y}_2]$, it is possible to obtain the zero-offset reflection traveltimes $t_0(\mathbf{Y},n)$ for all reflectors and the corresponding NMO velocities $V_{\mathrm{nmo}}(\alpha)$ (α is the azimuth). Input data also include the time slopes $\mathbf{p}(\mathbf{Y},n)=[p_1(\mathbf{Y},n),p_2(\mathbf{Y},n)]$ on the zero-offset (or stacked) section, where p_1 and p_2 are the horizontal slowness components of the zero-offset ray. The azimuthally-dependent NMO velocity is described by an elliptical function in the horizontal plane (Grechka and Tsvankin, 1998):

$$V_{\mathrm{nmo}}^{-2}(\alpha)=W_{11}\cos^2\alpha+2W_{12}\sin\alpha\cos\alpha+W_{22}\sin^2\alpha, \quad (1)$$

where $\mathbf{W}$ is a symmetric matrix,

$$W_{ij}=\tau_0\left.\frac{\partial^2\tau}{\partial x_i\,\partial x_j}\right|_{\mathbf{x}=\mathbf{Y}}, \quad (i,j=1,2). \quad (2)$$

Here $\tau(x_1,x_2)$ is the one-way traveltime from the zero-offset reflection point to the location $\mathbf{x}=\{x_1,x_2\}$ at the surface and τ_0 is the one-way zero-offset traveltime. The matrices $\mathbf{W}(\mathbf{Y},n)$ can be obtained from azimuthal velocity analysis based on the hyperbolic moveout equation parameterized by the NMO ellipse (Grechka and Tsvankin, 1999).

To model the effective NMO ellipse for a stack of TTI layers, we use the Dix-type averaging procedure devised by Grechka and Tsvankin (2002) for heterogeneous anisotropic media. They show that the exact NMO ellipse can be built by averaging the intersections of the interval NMO-velocity surfaces with the layer boundaries. All information for computing the NMO ellipse of a given reflection event is contained in the results of tracing just one (zero-offset) ray.

Because each layer is homogeneous with plane boundaries (Figure 1), it is sufficient to acquire the input data in a single multiazimuth CMP gather (Grechka et al., 2002b). The reflector depths $z_{\mathrm{b}}(n)$ are assumed to be measured in a borehole, which may be placed away from the CMP location (the subscript "b" denotes borehole data). Therefore, the vector of input data for 3D inversion is as follows:

$$\mathbf{d}=\{t_0(n),p_1(n),p_2(n),W_{11}(n),W_{12}(n),W_{22}(n),z_{\mathrm{b}}(n)\},\quad (n=1,2,\ldots,N), \quad (3)$$

where all components are the effective quantities for the nth reflector.

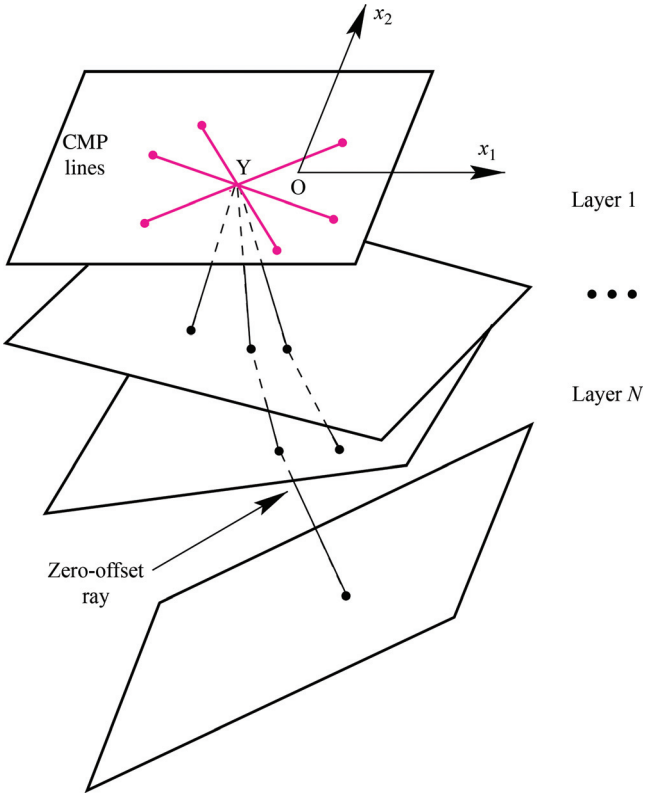

Figure 1. Zero-offset rays and a multiazimuth CMP gather for a stack of TTI layers separated by plane dipping interfaces (after Grechka et al., 2002b).

SYMMETRY AXIS ORTHOGONAL TO THE REFLECTOR

It is common to put constraints on the symmetry-axis orientation using a priori information (Charles et al., 2008; Huang et al., 2008; Bakulin et al., 2010). If TI layers were rotated by tectonic processes after sedimentation, the symmetry axis typically remains perpendicular to the layering, which means that its tilt ν and azimuth β coincide with the dip ϕ and azimuth ψ of the reflector, respectively. The relative simplicity of this model significantly improves the stability of parameter estimation.

Inversion for a single TTI layer

First, we consider a homogeneous TTI layer with the symmetry axis orthogonal to its bottom. The dip plane of the reflector represents a vertical symmetry plane for the whole model, and therefore, includes one of the axes of the NMO ellipse. Thus, the orientation of the NMO ellipse yields the reflector azimuth ψ which coincides with the symmetry-axis azimuth β.

The semiaxis of the NMO ellipse in the dip plane is obtained from the isotropic cosine-of-dip relationship (Tsvankin, 2005):

$$V_{\mathrm{nmo}}^{(1)}(\phi)=\frac{V_{\mathrm{nmo}}(0)}{\cos\phi}, \quad (4)$$

where $V_{\mathrm{nmo}}(0) = V_{\mathrm{P0}}\sqrt{1+2\delta}$ is the NMO velocity from a horizontal interface beneath a VTI medium with the same Thomsen parameters (i.e., the symmetry axis is rotated along with the reflector). Alternatively, the dip component of the NMO velocity can be represented using the ray parameter $p = \sqrt{p_1^2 + p_2^2}$:

$$V_{\mathrm{nmo}}^{(1)}(p) = \frac{V_{\mathrm{nmo}}(0)}{\sqrt{1 - p^2 V_{\mathrm{P0}}^2}}, \tag{5}$$

where $p = \sin\phi / V_{\mathrm{P0}}$ because the phase-velocity vector of the zero-offset ray (and the ray itself) is parallel to the symmetry axis. The strike component $V_{\mathrm{nmo}}^{(2)}$ of the NMO velocity is given by (Grechka and Tsvankin, 2000):

$$V_{\mathrm{nmo}}^{(2)} = V_{\mathrm{nmo}}(0) = V_{\mathrm{P0}}\sqrt{1+2\delta}. \tag{6}$$

Therefore, by combining the two semiaxes of the NMO ellipse (equations 5 and 6) and using the measured time slope p, one can find the symmetry-direction velocity V_{P0}. Then the dip $\phi = v$ is obtained from equation 4, and the anisotropy parameter δ from equation 6. Depth information for a single layer is not needed because the reflector depth z below the CMP location can be computed from the zero-offset traveltime t_0:

$$z = \frac{V_{\mathrm{P0}}\, t_0}{2\cos\phi}. \tag{7}$$

P-wave hyperbolic moveout in this model, however, is independent from the anisotropy parameter ε. In summary, the geometry and parameters V_{P0} and δ of a single TTI layer can be resolved from P-wave reflection traveltimes without using any borehole information.

Inversion for layered TTI media

Here, we present a 3D extension of the 2D stacking-velocity inversion algorithm of Wang and Tsvankin (2010) to layered TTI media. If the symmetry axis in each layer n is perpendicular to its bottom ($v^{(n)} = \phi^{(n)}$ and $\beta^{(n)} = \psi^{(n)}$), the model vector is

$$\mathbf{m} = \left\{ V_{\mathrm{P0}}^{(n)},\ \varepsilon^{(n)},\ \delta^{(n)},\ \phi^{(n)},\ \psi^{(n)} \right\}, \quad (n = 1, 2, \ldots, N). \tag{8}$$

Table 1. Interval parameters of a three-layer TTI model.

	Layer 1	Layer 2	Layer 3
V_{P0} (km/s)	1.5	2.0	2.5
ϵ	0.10	0.20	0.25
δ	−0.10	0.10	0.12

First, we assume the depths $z_{\mathrm{b}}(n)$ to be known (albeit with a certain error) from borehole measurements; later on, we discuss the inversion without using depth constraints.

Inversion methodology

We specify the trial set $\mathbf{m}$ of the interval parameters (equation 8) and trace zero-offset rays through the model with the geometry partially fixed by the known reflector depths. The ray-tracing results yield the zero-offset traveltimes $t_0^{\mathrm{calc}}(n)$, the horizontal slowness components $p_1^{\mathrm{calc}}(n)$ and $p_2^{\mathrm{calc}}(n)$, and the Dix-type averaging procedure produces the effective NMO ellipses $\mathbf{W}^{\mathrm{calc}}(n)$. The NMO velocity $V_{\mathrm{nmo}}^{\mathrm{calc}}(n,\alpha)$ for any azimuth α can be computed from equation 1.

The vector $\mathbf{m}$ is estimated by minimizing the following objective function (based on the L^2-norm) for all N reflectors simultaneously:

$$\mathcal{F}(\mathbf{m}) \equiv \sum_{n=1}^{N} \left\{ \frac{\left\| p_1^{\mathrm{calc}}(n) - p_1(n) \right\|^2}{\sigma^2[p_1(n)]} + \frac{\left\| p_2^{\mathrm{calc}}(n) - p_2(n) \right\|^2}{\sigma^2[p_2(n)]} + \frac{\left\| t_0^{\mathrm{calc}}(n) - t_0(n) \right\|^2}{\sigma^2[t_0(n)]} + \frac{\left\| V_{\mathrm{nmo}}^{\mathrm{calc}}(n,\alpha) - V_{\mathrm{nmo}}(n,\alpha) \right\|^2}{\sigma^2[V_{\mathrm{nmo}}(n,\alpha)]} \right\}, \tag{9}$$

where σ^2 represents the variance of each measurement, and the azimuth α varies from 0° to 180°. For 2D models, the objective function also includes check-shot traveltimes, and reflector dips are assumed to be known (Wang and Tsvankin, 2010). Here, wide-azimuth data provide additional information that replaces those borehole constraints.

In a single TTI layer, the parameter ε cannot be found from conventional-spread P-wave moveout. However, as discussed by Wang and Tsvankin (2010), the input parameters $\mathbf{p}(n)$, $t_0(n)$, and $\mathbf{W}(n)$ for layered TTI models are influenced by the values of $\varepsilon^{(n)}$ in the overburden (except for models with parallel interfaces). Therefore, the interval parameter ε is estimated along with the other unknowns, although typically it is not expected to be well-constrained.

Synthetic examples

The algorithm was tested for a suite of layered TTI models with a wide range of the anisotropy parameters ($0 \le \varepsilon \le 0.5$ and $-0.2 \le \delta \le 0.3$) and reflector dips between 0° and 60°. We used so-called trust-region-reflective optimization (Coleman and Li, 1996) to solve the nonlinear least-squares inverse problem defined by equation 9. Table 2 shows the inversion results for a three-layer medium with a wide range of interface azimuths (Table 1 and Figure 2). The results of a test for another three-layer

Table 2. Inversion results for the model from Table 1 and Figure 2. The input data are distorted by Gaussian noise with the standard deviations equal to 2% for $p_1(n)$, $p_2(n)$ and the NMO velocities, 1% for $t_0(n)$, and 0.2% for $z_{\mathrm{b}}(n)$. The mean values and standard deviations of the inverted parameters are denoted by "mean" and "sd," respectively.

	V_{P0} (km/s)		δ		ϵ		ϕ (°)		ψ (°)	
	mean	sd (%)	mean	sd	mean	sd	mean	sd	mean	sd
Layer 1	1.50	1	−0.10	0.01	0.09	0.05	30.0	0.4	0.0	0.1
Layer 2	2.00	3	0.10	0.03	0.20	0.08	30.0	0.5	45.1	1.5
Layer 3	2.51	5	0.12	0.06	0.23	0.24	30.0	0.6	90.2	2.4

medium with relatively close azimuths of the interfaces and large dips (Table 1 and Figure 3) are listed in Table 3. The inversion was performed for 200 realizations of noise-contaminated input data using the measurement values as the variances σ^2 in equation 9. Typically, the initial models were composed of horizontal isotropic layers with velocities sufficiently different (by 10% or more) from the exact values of V_{P0}. We also tested several initial models with nonzero reflector dips and found that the algorithm converged to the same global minimum.

For both models, the interval parameters V_{P0} and δ and the reflector dips and azimuths are recovered with sufficiently high accuracy. As expected, the standard deviations are higher in the third (deepest) layer (about 5% for V_{P0} and 0.06 for δ), primarily due to the smaller contribution of the deeper layers to the effective reflection traveltimes. However, in contrast to layer-stripping techniques, our tomography-style algorithm possesses the advantage of mitigating error accumulation with depth. An important factor that influences the inversion accuracy is the layer thickness; the thickness-to-depth ratio below the CMP location should reach at least 0.25 to ensure stable interval estimates. As expected, the standard deviations of the parameter ε are much larger than those of δ, although ε-estimates for the first model are not substantially biased.

For plausible ranges of ε and δ ($|\varepsilon| \le 0.5$; $|\delta| \le 0.3$), the errors in the interval parameters V_{P0}, δ, ϕ, and ψ remain small if the symmetry axis deviates from the reflector normal in the dip plane by less than 5° (i.e., $\beta = \psi$, but $\nu \neq \phi$). To evaluate the sensitivity to the difference between ν and ϕ, we changed the tilts for the second model (Table 1 and Figure 2; all dips are equal to 30°) to $\nu^{(n)} = 25°$ $(n = 1, 2, 3)$, generated the input data, and applied our algorithm assuming that $\nu^{(n)} = \phi^{(n)}$. The slight deviation of the symmetry axis from the reflector normal causes a mild bias in the estimates of V_{P0}, δ, ϕ, and ψ, but the

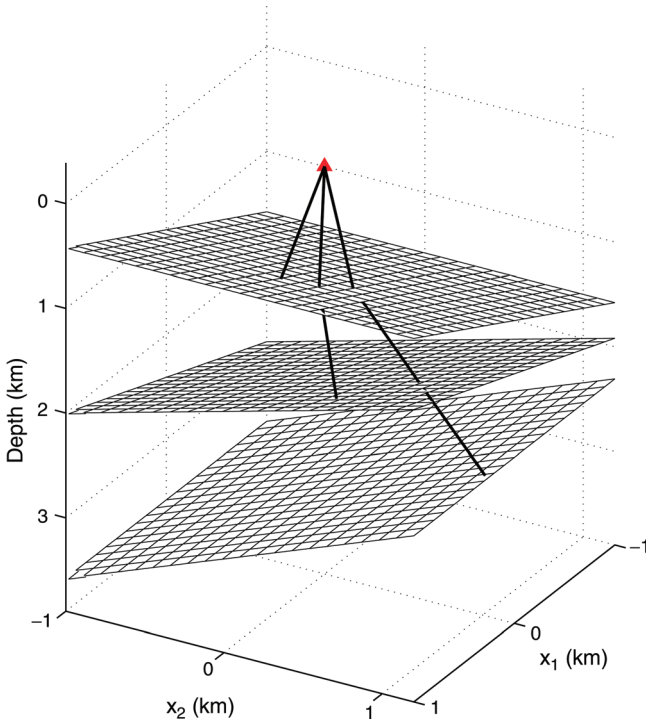

Figure 2. Zero-offset P-wave rays in a three-layer TTI model with the interval parameters listed in Table 1. The input data are computed by anisotropic ray tracing. The symmetry axis in each layer is perpendicular to its bottom. The dips and azimuths are $\phi^{(1)} = \phi^{(2)} = \phi^{(3)} = 30°$, $\psi^{(1)} = 0°$, $\psi^{(2)} = 45°$, and $\psi^{(3)} = 90°$. The reflector depths below the CMP (located at the origin of the coordinate system) are $z_b(1) = 1$ km, $z_b(2) = 2$ km, and $z_b(3) = 3$ km.

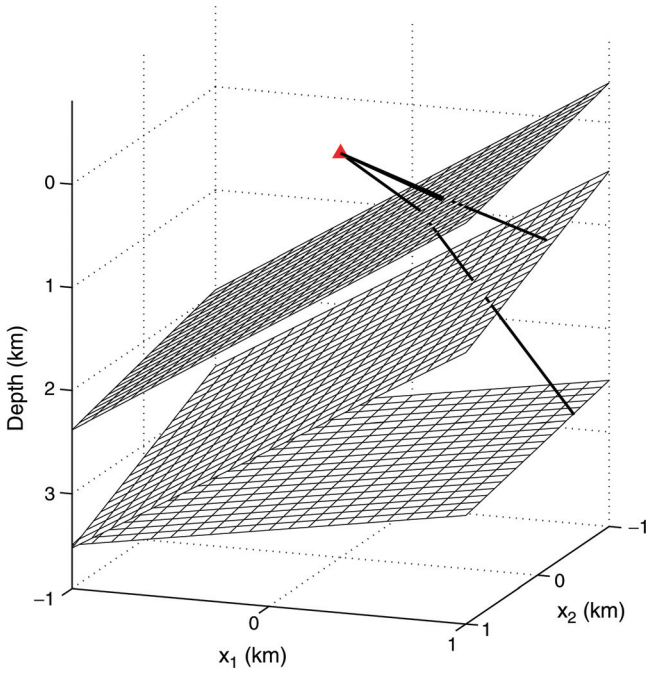

Figure 3. Zero-offset P-wave rays in a three-layer TTI model with the interval parameters listed in Table 1. The symmetry axis in each layer is perpendicular to its bottom. The dips and azimuths are $\phi^{(1)} = \phi^{(2)} = 50°$, $\phi^{(3)} = 20°$, $\psi^{(1)} = 10°$, $\psi^{(2)} = 20°$, and $\psi^{(3)} = 30°$. The reflector depths below the CMP are $z_b(1) = 1$ km, $z_b(2) = 2$ km, and $z_b(3) = 3$ km.

Table 3. Inversion results for the model from Table 1 and Figure 3. The noise level in the input data is the same as that in Table 2.

	V_{P0} (km/s)		δ		ϵ		ϕ (°)		ψ (°)	
	mean	sd (%)	mean	sd	mean	sd	mean	sd	mean	sd
Layer 1	1.50	1	−0.10	0.01	0.23	0.23	50.0	0.4	10.0	0.1
Layer 2	2.00	4	0.10	0.04	0.25	0.13	50.0	0.8	19.9	0.4
Layer 3	2.49	5	0.12	0.07	0.25	0.22	20.2	2.8	30.2	2.6

standard deviations are mostly controlled by the noise level, which is the same as in the previous tests.

If the reflector depths are also unknown, the trade-off between $z(n)$ and other parameters increases errors in the inversion results. For instance, we repeated the inversion for the model from Table 1 and Figure 2 without using depth information. For the same level of noise in the input data, the standard deviation of V_{P0} in the third layer increased from 5% (see Table 2) to 7% and in δ from 0.06 to 0.10. The estimated mean value of $z(3)$ (2.98 km) was almost unbiased with the standard deviation 0.11 km.

SYMMETRY AXIS DEVIATING FROM REFLECTOR NORMAL

As pointed out by Bakulin et al. (2010), the assumption of the symmetry axis being perpendicular to the reflector can become too restrictive when tectonic processes and sedimentation occur together. Also, for stress-induced anisotropy in sediments near salt bodies, the symmetry is largely controlled by the principal stress direction which is not necessarily aligned with the normal to the bedding.

To account for the deviation of the symmetry axis from the reflector normal, in some cases the tilt v can be expressed as a function of the dip ϕ using geologic data. For example, the simultaneous influence of tectonic forces and sedimentation typically makes v smaller than ϕ (e.g., $v=\phi/2$ or $v=3\phi/4$). In the next test, we used the three-layer model with the interval parameters listed in Table 1 and the model geometry shown in Figure 2, but with $v\neq\phi$. The symmetry axis in each layer is confined to the dip plane (i.e., $\beta^{(n)}=\psi^{(n)}$, $n=1,2,3$) with the tilt $v^{(n)}=\phi^{(n)}/2$. The known relationship between v and ϕ was sufficient for the algorithm to produce results (Table 4) similar to those for the symmetry axis orthogonal to the reflector (Table 2).

Tilt as an unknown parameter

Here, we relax the assumption that the tilt v represents a known function of the dip ϕ. It is still assumed that the symmetry-axis azimuth β in each layer coincides with the dip-plane azimuth ψ, but the parameter v has to be found from the data. Thus, the model vector includes one more unknown:

$$\mathbf{m}=\left\{V_{P0}^{(n)},\varepsilon^{(n)},\delta^{(n)},v^{(n)},\phi^{(n)},\psi^{(n)}\right\},\quad (n=1,2,\ldots,N). \tag{10}$$

Making v a free parameter significantly increases the nonuniqueness of the inversion. For 2D models, simultaneous estimation of V_{P0}, ε, δ, and v proves to be ambiguous, even if the reflector depths and dips are measured in a borehole. Our tests indicate that 3D wide-azimuth data supplemented by the known reflector depths still cannot be used to resolve the tilt along with the other TTI parameters. Therefore, we propose to add wide-azimuth walkaway VSP (vertical seismic profiling) traveltimes t_{VSP} to the vector $\mathbf{d}$ of input data:

$$\mathbf{d}=\{t_0(n),p_1(n),p_2(n),W_{11}(n),W_{12}(n),W_{22}(n),z_b(n),t_{VSP}\}. \tag{11}$$

The VSP data are excited by an array of sources at the surface and recorded by one receiver per layer located close to the layer's bottom. Similar to the zero-offset reflected rays, we trace VSP rays in a trial model and compute the difference between the modeled and observed traveltimes. Then the modified objective function takes the following form:

$$\mathcal{F}(\mathbf{m})\equiv\sum_{n=1}^{N}\left\{\frac{\left\|p_1^{calc}(n)-p_1(n)\right\|^2}{\sigma^2[p_1(n)]}+\frac{\left\|p_2^{calc}(n)-p_2(n)\right\|^2}{\sigma^2[p_2(n)]}+\frac{\left\|t_0^{calc}(n)-t_0(n)\right\|^2}{\sigma^2[t_0(n)]}+\frac{\left\|V_{nmo}^{calc}(n,\alpha)-V_{nmo}(n,\alpha)\right\|^2}{\sigma^2[V_{nmo}(n,\alpha)]}+\frac{\left\|t_{VSP}^{calc}-t_{VSP}\right\|^2}{\sigma^2[t_{VSP}]}\right\}. \tag{12}$$

Synthetic examples

Numerical testing shows that it is sufficient to add one checkshot source and several walkaway VSP sources located around the borehole with the offset exceeding 1/4 of the largest reflector depth. To achieve full azimuthal coverage, typically we place eight VSP sources along a circle with a 45° increment in azimuth. With the distribution of the VSP sources in Figure 4, we computed the input data for a three-layer model (Table 1 and Figure 5) using anisotropic ray tracing. The inversion results for 100 realizations of the noise-contaminated data are listed in Table 5. We also tested another model with the same geometry (Figure 5) but different tilts $v^{(1)}=30°$, $v^{(2)}=0°$, and $v^{(3)}=45°$ (Table 6).

As before, the initial models for the inversion were isotropic. However, if the tilt represents a free parameter, different inital guesses for reflector dips can lead to different inverted models corresponding to local minima of the objective function. Therefore, we ran the algorithm for several initial models with different interface dips and selected the result that provided the smallest data misfit. In practice, approximate dips picked on a depth image can serve as the initial guesses.

Despite the additional constraints provided by VSP data, the standard deviations in the tilt increase rapidly with depth because the inversion for v is still ill-conditioned. However, the interval parameters V_{P0} and δ and the reflector orientation can be well resolved despite a higher level of noise than that in the previous tests. Also, the VSP data help constrain the parameter ε in the top two layers, while estimation of ε in the bottom layer is ambiguous because of the poor angle coverage of the VSP rays at depth. To resolve the parameter ε in piecewise-homogeneous TTI models, it is necessary to use long-offset VSP or reflection data (Behera and Tsvankin, 2009).

Table 4. Inversion results for the model from Table 1 with the reflector geometry shown in Figure 2. The tilt of the symmetry axis in each layer is equal to one-half of the reflector dip (the symmetry axis lies in the dip plane). The noise level is the same as in the previous tests.

	V_{P0} (km/s)		δ		v (°)		ψ (°)	
	mean	sd (%)	mean	sd	mean	sd	mean	sd
Layer 1	1.50	1	−0.10	0.01	15.0	0.2	0.0	0.1
Layer 2	2.00	2	0.10	0.04	15.0	0.3	45.0	1.3
Layer 3	2.50	5	0.12	0.08	15.0	0.4	90.0	2.5

It should be mentioned that the deviation of the symmetry axis from the reflector normal reduces the stability of parameter estimation. When the difference between ν and ϕ is large, small errors in the input data can be significantly amplified by the inversion algorithm. Our numerical results indicate that the deviation of the symmetry axis from the reflector normal should not exceed 30°, which is typical for most TTI formations.

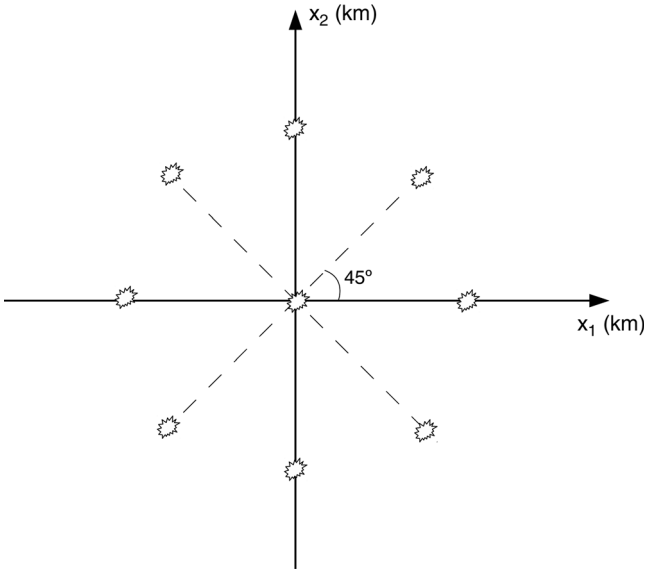

Figure 4. Distribution of VSP sources at the surface used for the model in Figure 5. The VSP lines are separated by 45°, and the offset of each VSP source is 1 km. The check-shot source is located close to the borehole ($x_1 = 0.01,\ x_2 = 0$).

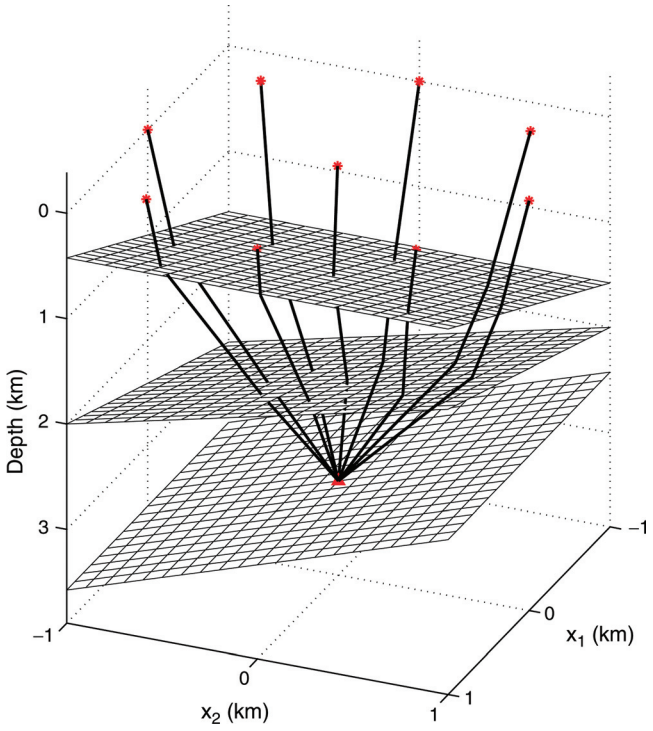

Figure 5. VSP rays for a receiver located at the bottom of a three-layer TTI model with the interval parameters listed in Table 1. The symmetry axis in each layer is confined to the dip plane. The tilts, dips, and azimuths are $\nu^{(1)} = \nu^{(2)} = \nu^{(3)} = 20°$, $\phi^{(1)} = \phi^{(2)} = \phi^{(3)} = 30°$, $\psi^{(1)} = 0°$, $\psi^{(2)} = 45°$, and $\psi^{(3)} = 90°$. The vertical borehole is below the coordinate origin, and the reflector depths at the borehole location are $z_b(1) = 1$ km, $z_b(2) = 2$ km, and $z_b(3) = 3$ km.

Table 5. Inversion results for the model from Table 1 and Figure 5 using reflection and VSP data. The positions of the check-shot and walkaway VSP sources are shown in Figure 4. The tilts are $\nu^{(1)} = \nu^{(2)} = \nu^{(3)} = 20°$. The input data are distorted by Gaussian noise with the standard deviations equal to 3% for $p_1(n)$ and $p_2(n)$, 2% for the NMO velocities, 1% for $t_0(n)$ and t_{VSP}^{calc}, and 0.5% for $z_b(n)$.

	V_{P0} (km/s)		δ		ϵ		ν (°)		ϕ (°)		ψ (°)	
	mean	sd (%)	mean	sd	mean	sd	mean	sd	mean	sd	mean	sd
Layer 1	1.50	1	−0.10	0.01	0.10	0.02	21.1	3.0	30.0	0.7	−0.1	0.4
Layer 2	2.00	2	0.09	0.04	0.21	0.06	20.5	5.5	30.0	0.9	45.3	1.2
Layer 3	2.48	3	0.13	0.06	0.25	0.13	24.9	11.4	30.1	0.9	90.0	1.3

Table 6. Inversion results using reflection and VSP data. The model is the same as in Table 5, except for the tilts $\nu^{(1)} = 30°$, $\nu^{(2)} = 0°$, and $\nu^{(3)} = 45°$.

	V_{P0} (km/s)		δ		ϵ		ν (°)		ϕ (°)		ψ (°)	
	mean	sd (%)	mean	sd	mean	sd	mean	sd	mean	sd	mean	sd
Layer 1	1.50	1	−0.10	0.01	0.10	0.02	29.7	2.6	29.9	0.7	0.0	0.5
Layer 2	1.99	1	0.11	0.03	0.21	0.03	1.7	2.4	30.1	0.9	44.8	1.0
Layer 3	2.52	3	0.11	0.06	0.30	0.09	40.7	11.5	29.9	1.0	89.9	1.4

CONCLUSIONS

The tilt of the symmetry axis makes the medium azimuthally anisotropic, and wide-azimuth P-wave data provide valuable constraints on the TTI parameters. If the symmetry axis is perpendicular to the reflector, the P-wave NMO ellipse is sufficient for estimating the parameters V_{P0} and δ of a single dipping TTI layer. Conventional-spread P-wave data also yield the depth and orientation of the reflector, but the parameter ε remains unconstrained without using long-offset (nonhyperbolic) moveout.

For homogeneous TTI layers separated by plane dipping interfaces, the input data include the effective NMO ellipses, zero-offset traveltimes, and reflection slopes supplemented by the reflector depths (presumably measured in a borehole). The interval parameters are estimated by a 3D tomography-style algorithm that represents an extension of the 2D method introduced in our previous publication. As long as the symmetry axis in each layer is kept orthogonal to its bottom, the interval parameters V_{P0} and δ and the reflector dips ϕ and azimuths ψ (and, therefore, the symmetry-axis orientation) are well-resolved. For models with common moderate values of the anisotropy parameters ($|\varepsilon| \leq 0.5$; $|\delta| \leq 0.3$), small deviations of the symmetry axis from the reflector normal ($\leq 5^\circ$) do not substantially distort the inversion results. If depth information is not available, the model parameters are estimated with larger bias and standard deviation.

We also examined the possibility of extending the inversion to models in which the symmetry axis deviates from the reflector normal but is confined to the dip plane. If the relationship between the symmetry-axis tilt and reflector dip in each layer is known, the algorithm can still resolve the interval parameters V_{P0} and δ along with the interface orientation. However, when tilt represents a free parameter, stable inversion requires additional input data, such as check-shot and walkaway VSP traveltimes. VSP data should have full azimuthal coverage, and the distance between the VSP sources and the borehole has to reach 1/4 of the largest reflector depth. Another essential requirement is for the angle between the symmetry axis and reflector normal not to exceed 30°. Depending on the offset coverage of VSP data, it may be possible to constrain the parameter ε in the shallow part of the section. The addition of walkaway VSP data can also increase the accuracy of the inversion for models with the symmetry axis orthogonal to the reflector.

ACKNOWLEDGMENTS

We are grateful to Vladimir Grechka (Shell) and Andres Pech (IPN, Mexico) for making available their codes. We also thank Andrey Bakulin (Saudi Aramco), Paul Fowler (WesternGeco), Ken Larner (CWP), and the reviewers of *Geophysics* for numerous helpful suggestions. This work was supported by the Consortium Project on Seismic Inverse Methods for Complex Structures at CWP.

REFERENCES

Bakulin, A., M. Woodward, D. Nichols, K. Osypov, and O. Zdraveva, 2010, Building tilted transversely isotropic depth models using localized anisotropic tomography with well information: Geophysics, **75**, no. 4, D27–D36, doi:10.1190/1.3453416.

Behera, L., and I. Tsvankin, 2009, Migration velocity analysis for tilted transversely isotropic media: Geophysical Prospecting, **57**, 13–26, doi:10.1111/j.1365–2478.2008.00732.x

Charles, S., D. R. Mitchell, R. A. Holt, J. Lin, and J. Mathewson, 2008, Data-driven tomographic velocity analysis in tilted transversely isotropic media: A 3D case history from the Canadian Foothills: Geophysics, **73**, no. 5, VE261–VE268, doi:10.1190/1.2952915.

Coleman, T. F., and Y. Li, 1996, An interior trust region approach for nonlinear minimization subject to bounds: SIAM Journal on Optimization, **6**, no. 2, 418–445, doi:10.1137/0806023.

Grechka, V., A. Pech, and I. Tsvankin, 2002a, Multicomponent stacking-velocity tomography for transversely isotropic media: Geophysics, **67**, 1564–1574, doi:10.1190/1.1512802.

———, 2002b, P-wave stacking-velocity tomography for VTI media: Geophysical Prospecting, **50**, no. 2, 151–168, doi:10.1046/j.1365–2478.2002.00307.x.

Grechka, V., A. Pech, I. Tsvankin, and B. Han, 2001, Velocity analysis for tilted transversely isotropic media: A physical-modeling example: Geophysics, **66**, 904–910, doi:10.1190/1.1444980.

Grechka, V., and I. Tsvankin, 1998, 3D description of normal moveout in anisotropic inhomogeneous media: Geophysics, **63**, 1079–1092, doi:10.1190/1.1444386.

Grechka, V., and I. Tsvankin, 1999, 3D moveout inversion in azimuthally anisotropic media with lateral velocity variation: Theory and a case study: Geophysics, **64**, 1202–1218, doi:10.1190/1.1444627.

———, 2000, Inversion of azimuthally dependent NMO velocity in transversely isotropic media with a tilted axis of symmetry: Geophysics, **65**, 232–246, doi:10.1190/1.1444714.

———, 2002, NMO-velocity surfaces and Dix-type formulas in anisotropic heterogeneous media: Geophysics, **67**, 939–951, doi:10.1190/1.1484536.

Huang, T., S. Xu, J. Wang, G. Ionescu, and M. Richardson, 2008, The benefit of TTI tomography for dual azimuth data in Gulf of Mexico: 78th Annual International Meeting, SEG, Expanded Abstracts, 222–226.

Isaac, J. H., and D. C. Lawton, 1999, Image mispositioning due to dipping TI media: A physical seismic modeling study: Geophysics, **64**, 1230–1238, doi:10.1190/1.1444629.

Neal, S. L., N. R. Hill, and Y. Wang, 2009, Anisotropic velocity modeling and prestack Gaussian-beam depth migration with applications in the deepwater Gulf of Mexico: The Leading Edge, **28**, 1110–1119, doi:10.1190/1.3236381.

Thomsen, L., 1986, Weak elastic anisotropy: Geophysics, **51**, 1954–1966, doi:10.1190/1.1442051.

Tsvankin, I., 2005, Seismic signatures and analysis of reflection data in anisotropic media, 2nd edition: Elsevier Science Publishing Co., Inc.

Vestrum, R. W., D. C. Lawton, and R. Schmid, 1999, Imaging structures below dipping TI media: Geophysics, **64**, 1239–1246, doi:10.1190/1.1444630.

Wang, X., and I. Tsvankin, 2010, Stacking-velocity inversion with borehole constraints for tilted TI media: Geophysics, **75**, no. 5, D69–D77, doi:10.1190/1.3481652.